SolarPACES 2023, 29th International Conference on Concentrating Solar Power, Thermal, and Chemical Energy Systems

Analysis and Simulation of CSP and Hybridized Systems

https://doi.org/10.52825/solarpaces.v2i.804

Published: 15 Oct. 2024

Time-Dependent Failure Assessment of Ceramic Receivers

Bipul Barua[1], Pawan Chaugule[1], Mark C. Messner[1], and Dileep Singh[1]

[1] Argonne National Laboratory, United States of America

* Correspondence: Bipul Barua, barua@anl.gov

Abstract. The outlet temperature targets for Gen 3 Concentrating Solar Power (CSP) systems pose a significant challenge to the structural reliability of high temperature metallic components, including those manufactured from nickel-based superalloys. Advanced ceramics present a potential solution due to their excellent high-temperature strength. However, accurate assessment of ceramic components requires an entirely different approach compared to metallic components. This paper describes the implementation of time-dependent reliability analysis of ceramic components in *srlife* – an open-source software package for estimating the life of high temperature CSP components. This new capability will allow high temperature CSP designers to make fair comparisons between competing metallic and ceramic designs and accurately assess the performance of different ceramic materials for CSP receivers and other components. The current version of the tool is available at https://github.com/Argonne-National-Laboratory/srlife.

Keywords: Ceramics, Reliability, High Temperature Design, Solar Receivers

1. Introduction

Achieving the SunShot initiative's 2030 LCOE target for concentrating solar power (CSP) systems requires high efficiency, high temperature solar receivers providing heat transfer fluid (HTF) with outlet temperatures exceeding 700° C [1]. Previous research [2], [3] suggests designing such receivers using current-generation nickel-based alloys will be extremely challenging. Ceramic materials, with their excellent creep and dwell fatigue properties at high temperature and low coefficient of thermal expansion, might be a viable solution [4], [5]. However, there is currently a lack of suitable methods and software tools for designing high-temperature receivers, which precludes detailed comparison between metallic and ceramic receiver concepts.

Ceramic materials exhibit fundamentally different failure mechanisms compared to metals [5], [6], [7]. Ceramic structures inherently contain subscale flaws originated from the manufacturing process. These flaws can undergo unstable growth under thermal and mechanical loads and can reach a critical size, leading to catastrophic failure of the component. This indicates that failure in ceramics primarily occurs through brittle fracture processes. At higher scale, this can be described using a statistical failure theory based on a size dependent probability distribution. Given the size-dependent failure distribution, often generated by fitting experimental strength data to Weibull distribution, along with a correlation that accounts for stress multiaxiality, such as via Weibull's classical model [8] or Batdorf's theory [9], the stress analysis results can be utilized to determine the probability of time-independent, fast fracture failure in a ceramic component. The CARES program [6], [7], developed by NASA, provides a comprehen-

sive implementation of this approach for time-independent, fast fracture design analysis. Recently, we have incorporated the time-independent ceramic reliability analysis into *srlife* [10], [11], [12], an open-source tool originally designed for estimating the life of metallic receivers [13], [14], [15].

The pre-existing subscale flaws in ceramics can also grow under cyclic loading, a phenomenon known as subcritical crack growth (SCG) [7]. During the initial cycle, the component may not necessarily fail, but with repeated fatigue loading, the original flaw distribution changes as flaw sizes increase over time. Eventually, this initial flaw distribution can grow to a point where the component has a high probability of failure through time-independent rapid fracture. The CARES program addresses this subcritical crack growth by adapting the material's Weibull distribution to align with the current flaw distribution. This time-dependent failure analysis follows the same approach as in the time-independent analysis but uses an increased effective stress distribution to account for the increase in probability of failure due to the SCG.

In this paper, we present the implementation of the time-dependent failure analysis for ceramic receivers within *srlife*. This implementation includes volume and surface flaw reliability analyses, utilizing various models that are independent of crack shape, as well as models that account for crack shape dependencies. These models include both shear-sensitive and shear-insensitive fracture criteria, all sourced from the CARES program [7].

2. Ceramic Failure Models

The ceramic failure models implemented in *srlife* are based on different failure criteria [6], [7] including – (i) the principal of independent action (PIA) method, (2) Weibull normal tensile stress averaging (WNTSA) method, (3) maximum tensile stress (MTS) criterion, (4) total coplanar strain energy (CSE) release rate criterion, and (5) Shetty's mixed mode (SMM) criterion. The PIA and WNSTA models are inherently crack shape independent and shear insensitive, while other models are crack shape dependent. *srlife* provides options for modelling two types of cracks – Griffith flaw (GF) and penny-shaped flaw (PSF) – for volume flaw reliability analysis and another two types – Griffith notch (GN) and Semi-circular crack (SCC) – for surface flaw analysis. For the four crack shape dependent models, *srlife* provides two analysis options – one using shear insensitive fracture criteria and one using shear sensitive fracture criteria. Table 1 lists all the models implemented in *srlife* and specifies their relevance for various types of analysis options.

Table 1. *Reliability models and available analysis options.*

Model		Crack type	Shear insensitive fracture criteria		Shear sensitive fracture criteria	
			Volume flaw	Surface flaw	Volume flaw	Surface flaw
Crack shape independent	PIA	-	yes	yes	no	no
	WNTSA	-	yes	yes	no	no
Crack shape dependent	MTS	GF	yes	yes	yes	yes
		PSF	yes	no	yes	no
	SMM	GF	yes	yes	yes	yes
		PSF	yes	no	yes	no
		GN	no	yes	no	yes
		SCC	no	yes	no	yes
	CSE	GF	yes	yes	yes	yes
		PSF	yes	no	yes	no
		GN	no	yes	no	yes

Tables 2 and 3 list the constitutive equations for time-dependent probability of failure specific to volume flaws and surface flaws, respectively. Determining the time-dependent failure

probability requires transforming the effective stress distribution at time, $t = t_f$ to its equivalent stress distribution at time, $t = 0$. These transformation equations consist of two parts: the first part involves time integration of effective stress to account for the evolution of crack distribution due to SCG, while the second part addresses the initial distribution of flaws. The first part of the equations diminishes when $t_f = 0$, resulting in the transformed effective stress becoming the effective stress used for time-independent failure analysis. The effective stress for PIA model is a combination of the principal stresses. For the WNTSA model, it represents the normal tensile stress averaged over the surface of a unit-radius sphere in volume flaw analysis and averaged over the contour of a unit radius circle in surface flaw analysis. In contrast, all the crack shape dependent models employ a combination of normal and shear stresses, following the equations listed in Table 4. Details of the development of these time-dependent ceramic failure models can be found in the CARES manual [7].

***Table 2**. Time-dependent failure models specific to volume flaws.*

Model	Probability of failure	Transformed effective stress
PIA	$P_{fV}(t_f) = 1 - exp\left[-k_{wV}\int_V \sum_{i=I}^{III} \sigma_{i,0}\, dV\right]$ (1) where, k_{wV} is the uniaxial Weibull crack density coefficient for volume flaws and t_f is the service life.	$\sigma_{i,0} = \left[\frac{\int_0^{t_f} \sigma_i^{N_V}(t)dt}{B_V} + \sigma_i^{N_V-2}(t_f)\right]^{\frac{1}{N_V-2}}$ (2) where, σ_i's are the principal tensile stresses, B_V and N_V are material parameters.
WNTSA	$P_{fV}(t_f) = 1 - \exp\left[-k_{wpV}\int_V \bar{\sigma}_{n,0}^{m_V} dV\right]$ (3) where, k_{wpV} is the polyaxial Weibull crack density coefficient for volume flaws.	$\bar{\sigma}_{n,0} = \left[\frac{\int_0^{t_f} \bar{\sigma}_n(t)dt}{B_V} + \bar{\sigma}_n(t_f)\right]^{\frac{1}{N_V-2}}$ (4) where, $\bar{\sigma}_n$ is the average normal tensile stress.
MTS, CSE, SMM	$P_{fV}(t_f) = 1 - \exp\left[-\frac{k_{BV}}{2\pi}\int_V \int_0^{2\pi} \int_0^{\frac{\pi}{2}} \sigma_{e,0}^{-m_V} sin\alpha\, d\alpha\, d\beta\, dV\right]$ (5) where, k_{BV} is the Batdorf crack density coefficient for volume flaws.	$\sigma_{e,0} = \left[\frac{\int_0^{t_f} \sigma_e^{N_V}(t)dt}{B_V} + \sigma_e^{N_V-2}(t_f)\right]^{\frac{1}{N_V-2}}$ (6) where σ_e is the effective stress.

***Table 3**. Time-dependent failure models specific to surface flaws.*

Model	Probability of failure	Transformed effective stress
PIA	$P_{fS}(t_f) = 1 - \exp\left[-k_{wS}\int_A \sum_{i=I}^{II} \sigma_{i,0}\, dA\right]$ (7) where, k_{wS} is the uniaxial Weibull crack density coefficient for surface flaws and t_f is the service life.	$\sigma_{i,0} = \left[\frac{\int_0^{t_f} \sigma_i^{N_S}(t)dt}{B_S} + \sigma_i^{N_S-2}(t_f)\right]^{\frac{1}{N_S-2}}$ (8) where, σ_i's are the principal tensile in-plane stresses acting on the surface of the structure, B_S and N_S are material parameters.
WNTSA	$P_{fS}(t_f) = 1 - \exp\left[-k_{wpS}\int_A \bar{\sigma}_{n,0}^{m_S} dA\right]$ (9) where, k_{wpV} is the polyaxial Weibull crack density coefficient for surface flaws.	$\bar{\sigma}_{n,0} = \left[\frac{\int_0^{t_f} \bar{\sigma}_n(t)dt}{B_S} + \bar{\sigma}_n(t_f)\right]^{\frac{1}{N_S-2}}$ (10) where, $\bar{\sigma}_n$ is the average normal tensile stress.
MTS, CSE, SMM	$P_{fS}(t_f) = 1 - \exp\left[-\frac{k_{BS}}{\pi}\int_A \int_0^{\pi} \sigma_{e,0}^{-m_S}\, d\alpha\, dA\right]$ (11) where, k_{BS} is the Batdorf crack density coefficient for surface flaws.	$\sigma_{e,0} = \left[\frac{\int_0^{t_f} \sigma_e^{N_S}(t)dt}{B_V} + \sigma_e^{N_S-2}(t_f)\right]^{\frac{1}{N_S-2}}$ (12) where, σ_e is the effective stress.

***Table 4**. Effective stress, σ_e for various crack shape dependent models.*

Crack Shape	Model		
	MTS	**CSE**	**SMM**
GF	$\frac{1}{2}\left(\sigma_n + \sqrt{\sigma_n^2 + \tau^2}\right)$ (13)	$\sqrt{\sigma_n^2 + \tau^2}$ (14)	$\frac{1}{2}\left(\sigma_n + \sqrt{\sigma_n^2 + 4\left(\frac{\tau}{\bar{C}}\right)^2}\right)$ (15)
PSF	$\frac{1}{2}\left(\sigma_n + \sqrt{\sigma_n^2 + \left[\frac{\tau}{1-0.5\nu}\right]^2}\right)$ (16)	$\frac{1}{2}\left(\sqrt{\sigma_n^2 + \left[\frac{\tau}{1-0.5\nu}\right]^2}\right)$ (17)	$\frac{1}{2}\left(\sigma_n + \sqrt{\sigma_n^2 + \left(\frac{4\tau}{\bar{C}(2-\nu)}\right)^2}\right)$ (18)
GN		$\frac{1}{2}\left(\sqrt{\sigma_n^2 + \frac{0.7951}{1-\nu}\tau^2}\right)$ (19)	$\frac{1}{2}\left(\sigma_n + \sqrt{\sigma_n^2 + 3.1803\left(\frac{\tau}{\bar{C}}\right)^2}\right)$ (20)
SCC			$\frac{1}{2}\left(\sigma_n + \sqrt{\sigma_n^2 + 3.301\left(\frac{\tau}{\bar{C}}\right)^2}\right)$ (21)
where, $\sigma_n = \sigma_1 l^2 + \sigma_2 m^2 + \sigma_3 n^2$ (22) for volume flaws and $\sigma_n = \sigma_1 l^2 + \sigma_2 m^2$ (23) for surface flaws, and $\tau = \sigma^2 - \sigma_n^2$, with σ_n being the normal stress, τ the shear stress, σ the traction vector acting on the crack plane, l, m, n the direction cosine and ν is poisson's ratio. $\bar{C}$ in SMM model is an empirical constant determined from experimental data.			

3. Validation of Model Implementation in *srlife*

We validated the implementation of the ceramic time-dependent failure models in *srlife* by simulating an example problem provided in the CARES manual [7]. This problem involved a silicon nitride annular disc with specific dimensions (3.8 mm thickness, 82.55 mm outer diameter, and 12.7 mm inner diameter) subjected to various constant and cyclic angular speeds. We performed finite element analysis of the disc to determine the stresses under the applied loading conditions.

The stress results obtained from finite element analysis were then fed into *srlife*'s reliability calculator. Failure probabilities of the disc were determined for various loading conditions as a function of service life using different failure models. The comparison of the failure probabilities calculated by *srlife* with the documented results in the CARES manual revealed a close match. Figure 1 shows example comparisons showing results for two constant loading conditions (angular speeds: 60,000 rpm and 80,000 rpm) as well as for a cyclic loading condition (angular speeds sinusoidally varied between 60,000 rpm and 80,000 rpm) using the SMM model for PSF crack shape.

4. Evaluating Reliability of a Ceramic Receiver

Figure 2 outlines the general process of evaluating a ceramic receiver using *srlife*. The user provides the tube dimensions (height, outer diameter, and thickness), number of tubes in each panel, panel arrangements in each flowpath, mass flow rates for the HTF in each flowpath, the net incident heat flux and pressure as functions of time for each tube considered in analysis. To reduce the cost of the analysis the user can analyze a limited subset of representative tubes from each panel. *srlife* includes a simple thermohydraulic analysis module that computes the heat balance in each flow path in the receiver. The fluid mass flow rate can either be constant, which results in variable fluid outlet temperatures, or a function of time to maintain a consistent

fluid outlet temperature throughout the day. For the latter option, the mass flow rates at different times of the day can be determined iteratively using the thermohydraulic solver. *srlife* then employs the structural analysis modules to determine the stress and strain fields using the internal pressure and the temperature results from the thermohydraulic analysis.

At this stage, the software has calculated stress and temperature profiles for each tube in the receiver. The final step is then to convert these results into reliability. *srlife* utilizes the equations provided in Tables 2, 3, and 4 to calculate reliability of each tube using the stress field and the temperature dependent material properties. Details of the *srlife* development and its various modules can be found in [10], [13], [14].

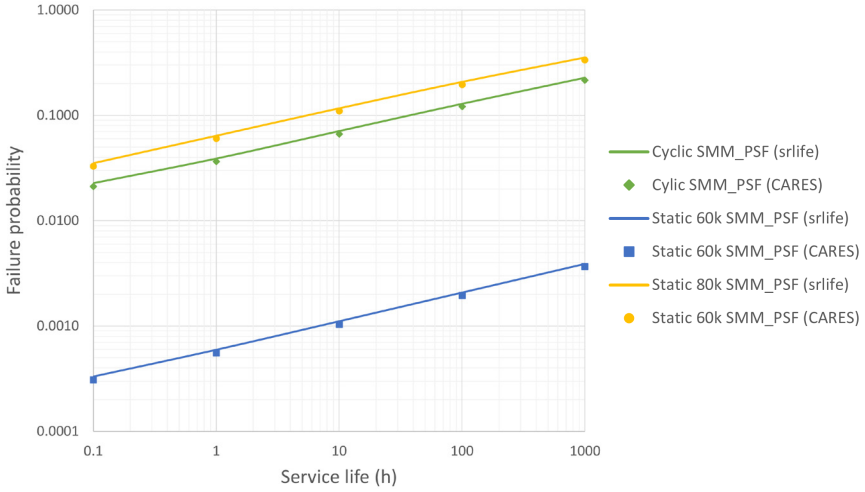

Figure 1. *Failure probability results compared between srlife and CARES program for an annular disc.*

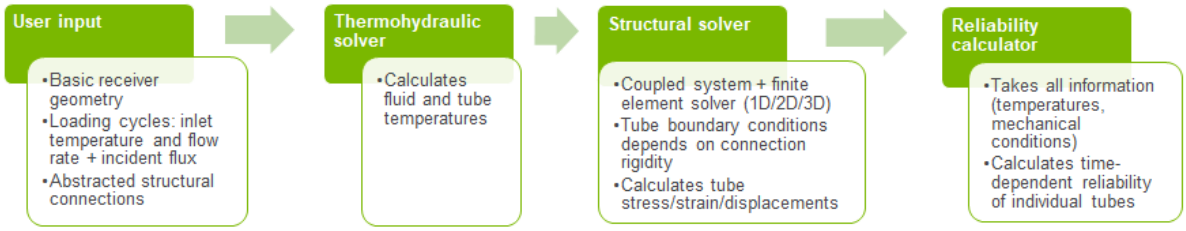

Figure 2. *Flow chart illustrating analysis steps in reliability evaluation.*

5. Example Problem

We performed time-dependent reliability analysis of a CSP reference receiver model to assess the implementation of different time-dependent failure models of ceramics in *srlife*. The reference receiver model is a 21 m tall, 18 m diameter, 360° external cylindrical receiver with a thermal design power of 500 MW_t and maximum net heat flux of 750 kW/m^2. Figure 3(a) shows the radiation heat map on the receiver at noon and Figure 3(b) plots the variation in heat flux during the day. Since the heat flux map is symmetric about the north-south axis, we considered two serpentine flow paths, each containing six panels for the HTF. The HTF enters the receiver at the north side through Panel-1 and leaves the receiver at the south side through Panel-6. Each panel consists of 100 tubes with 42.2 mm outer diameter and 3 mm thickness. We considered chloride salt as the HTF for the receiver. The HTF inlet and outlet temperatures are 550°C and 720°C, respectively. The tube material is SiC. All the required material properties for SiC are taken from CAREs manual [7].

We performed thermohydraulic analysis of the reference receiver considering two representative tubes – one with the highest heat flux and one with the lowest heat flux – from each

panel and considering a panel weight factor of 50 for each tube. We considered variable mass flow rates for the reference receiver. The mass flow rate at each time step was optimized in an iterative manner so that the fluid outlet temperature is always about 720°C. Figure 3(c) plots the fluid temperature and tube crown temperature along the flow path from the start of day to noon for the two tubes considered in analysis. Figure 4(a) plots the tube outer wall temperature distribution at noon for the hottest tube in each panel.

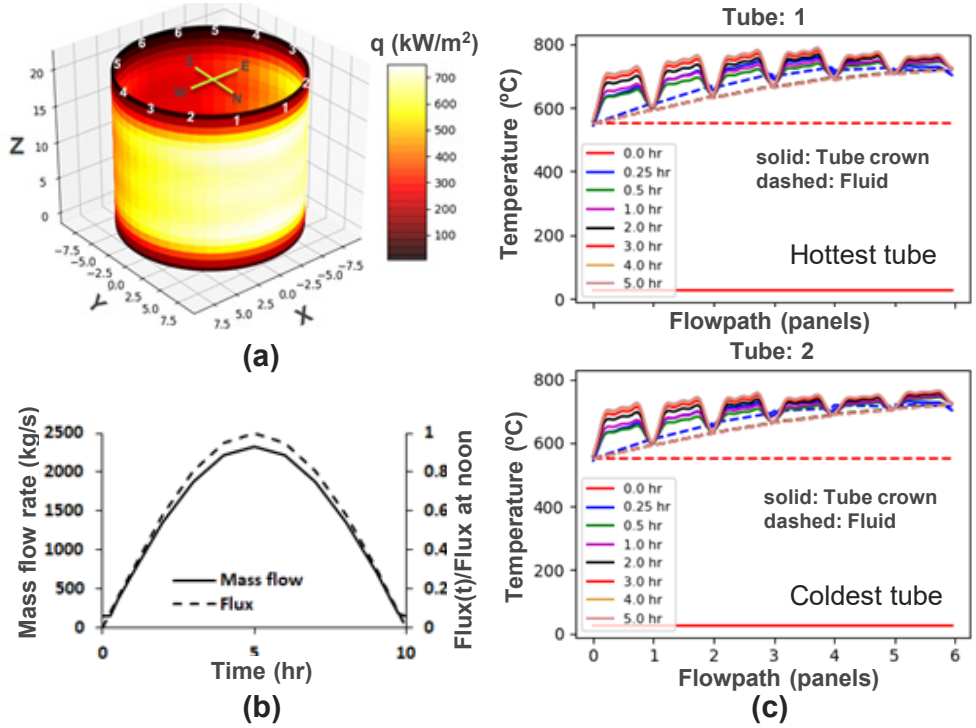

Figure 3. *(a) Heat flux map on the receiver at noon, (b) variation in heat flux and HTF mass flow rate during the day, (c) changes in HTF and tube crown temperatures (shown for the hottest and coldest tubes) along a flow path from the start of the day to noon.*

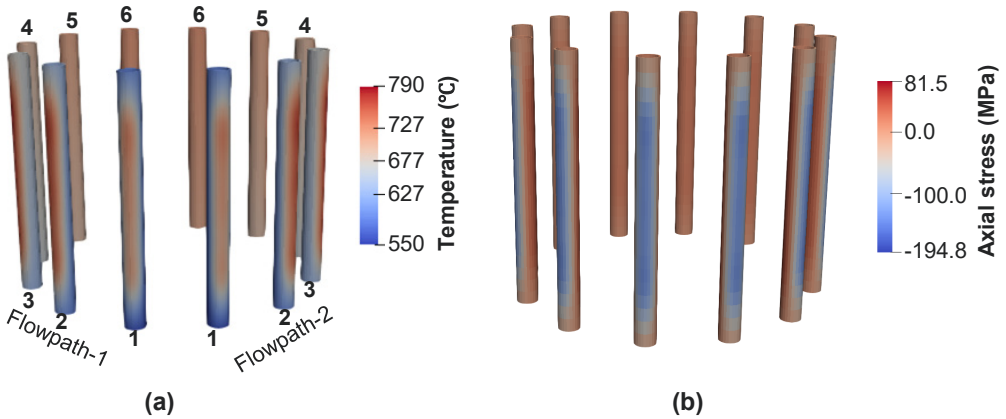

Figure 4. *(a) Temperature and (b) axial stress distribution in the hottest tube of each panel at noon.*

Using the temperature results from thermohydraulic analysis and design fluid pressure determined based on a simple pressure loss calculation, we performed the structural analysis of the receiver. The design fluid pressure is 3.2 MPa. For structural analysis we considered the tubes in a panel are rigidly connected to the tube manifold but the panels are mechanically disconnected from each other. Figure 3(b) plots the axial stress distribution at noon for the hottest tube in each panel. The reliability module of *srlife* then performs time-dependent reliability analysis using the stress results from structural analysis and for a given service life. The results are reliability of individual tubes considered in analysis.

Figure 5 plots the minimum tube reliability as a function of time for volume flaw, surface flaw, and combined volume and surface flaw. These reliabilities were calculated using PIA model. For all the cases, the reliability decrease as the service life increases, indicating correct implementation of the time-dependent reliability analysis in *srlife*. Figure 6 compares the minimum tube reliability calculated by various failure models and flaw types for a service life of 10,000 days (~ 30 years). Results are shown from volume flaw analysis, surface flaw analysis, and combined volume and surface flaw analysis for the respective suitable models and flaw types as listed in Table 1.

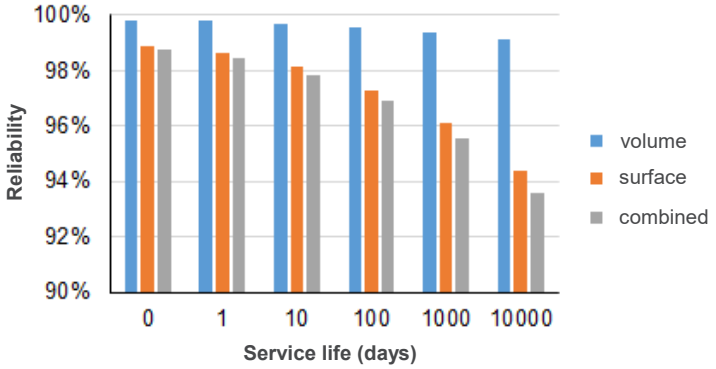

Figure 5. *Minimum tube reliability as a function of service life using the PIA model.*

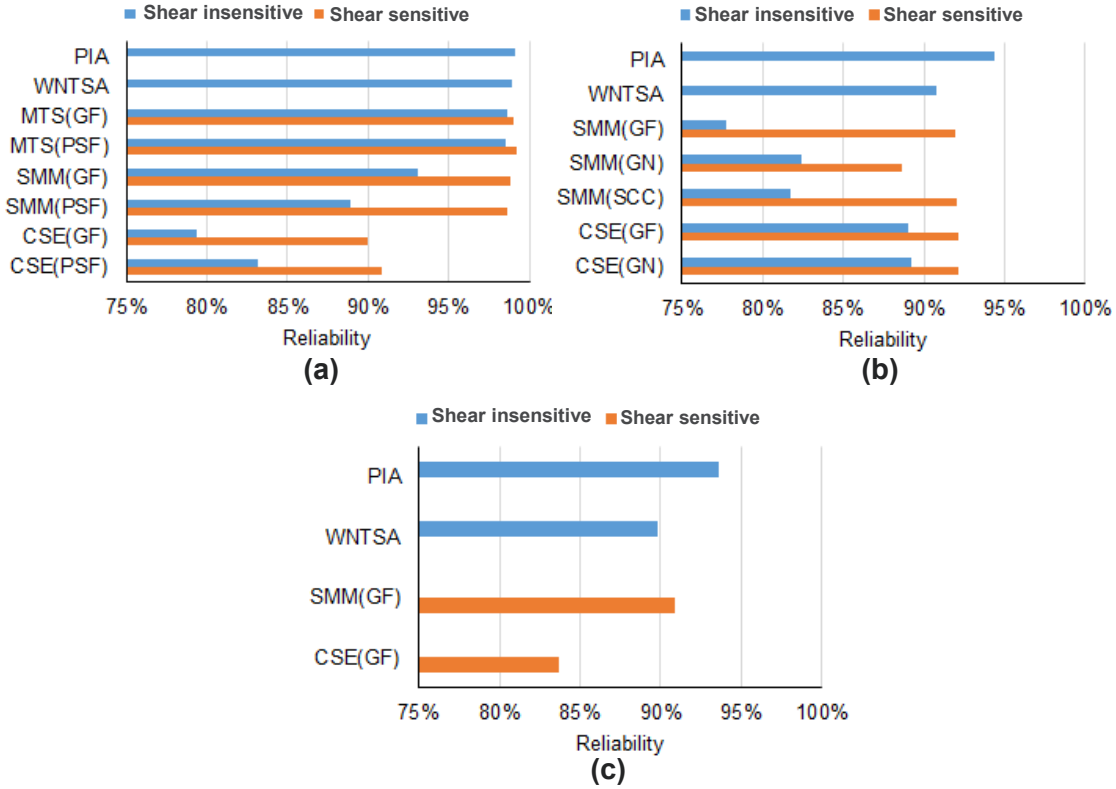

Figure 6. *Minimum tube reliability versus failure model for a service life of 10,000 days (~ 30 years). (a) Volume flaw reliability, (b) surface flaw reliability, (c) combined volume and surface flaw reliability.*

The conservatism in the models for volume flaw analysis aligns with our previous observation from time-independent volume flaw analysis of a reference receiver model [12]. A comparison between shear-sensitive and shear-insensitive analyses using the Batdorf model (MTS, CES, SMS) suggests that employing shear-insensitive fracture criteria results in lesser reliability prediction compared to the use of shear-sensitive fracture criteria. This is attributed to the larger value of the Batdorf crack density coefficient for shear-insensitive fracture criteria than for shear-sensitive criteria. For surface flaw reliability, the GN predicts less reliability than

the GF, which is expected. The reliability prediction for SCC is in between the GN and GF.

6. Conclusions

We extended the capability of the open-source software package, *srlife*, to perform time-dependent reliability analysis of ceramic components. We demonstrated the new capability by evaluating a SiC ceramic tubular panel receiver for a variety of ceramic failure models and crack shapes. The software, including the underlying material data, is available for use by the community under an open-source license (see data availability below). The package can be used to evaluate specific designs, with the goal of aiding industry in optimizing plant design, and to make broad assessments of the viability and effectiveness of a wide variety of material types, covering both metals and ceramics, when applied to high temperature CSP receivers and other components.

Data availability statement

The material data used in the sample problem is contained in the distribution of the *srlife* software, available at https://github.com/Argonne-National-Laboratory/srlife.

Underlying and related material

The source code for *srlife* and the input data for various examples are available at https://github.com/Argonne-National-Laboratory/srlife.

Author contributions

B. B. contributed to the initial and final drafts of the manuscript and ran the example analysis. M. C. M. modified the *srlife* software. P. C. added the ceramic failure models to *srlife*. M. C. M. and D. S. helped administer the project. All reviewed and edited the final manuscript.

Competing interests

The authors declare no competing interests.

Funding

This work was sponsored by the U.S. Department of Energy, under Contract No. DE-AC02-06CH11357 with Argonne National Laboratory, managed and operated by UChicago Argonne LLC. The authors gratefully acknowledge support from the U.S. Department of Energy through the Office of Energy Efficiency and Renewable Energy, Solar Energy Technologies Office, CSP Program (project 38482).

References

[1] M. Mehos, et al. “Concentrating solar power Gen3 demonstration roadmap.” National Renewable Energy Laboratory technical report NREL/TP-5500-67464, 2017.
[2] B. Barua, and M. C. Messner. “Structural design challenges and implications for high temperature concentrating solar power receivers.” Solar Energy 251 (2023): 119-133.
[3] B. Barua, et al. “Design Guidance for High Temperature Concentrating Solar Power Components.” Argonne National Laboratory technical report ANL-20/03, 2020. (https://doi.org/10.2172/1582656)
[4] B. Barua et al. “Assessment of Ti3SiC2 MAX phase as a structural material for high temperature receivers”. In *AIP Conference Proceedings* (Vol. 2445, No. 1). AIP Publishing, 2022.

[5] M. C. Messner et al. “Towards a Design Framework for Non-metallic Concentrating Solar Power Components.” In the Proceedings of the 2021 SolarPACES Conference, 2021.
[6] N. N. Nemeth, et al. “Ceramics Analysis and Reliability Evaluation (CARES) Users and Programmers Manual,” 1990.
[7] N.N Nemeth, et al. CARES/LIFE ceramics analysis and reliability evaluation of structures life prediction program. No. NASA/TM-2003-106316. 2003.
[8] Weibull, W. A. “The phenomenon of rupture in solids.” *IVA Handlingar*, 153, 1939.
[9] S. B. Batdorf, and J.G. Crose, “Statistical Theory for the Fracture of Brittle Structures Subjected To Nonuniform Polyaxial Stresses.” Journal of Applied Mechanics, 459–464, 1974.
[10] Messner, Mark, et al. "A Computer Design Tool for Ceramic Receivers." *SolarPACES Conference Proceedings*. Vol. 1. 2022.
[11] P. Chaugule, et al., “*Design Methods, Tools, and Data for Ceramic Solar Receivers Year 1 Continuation Report,”* (No. ANL-22/48). Argonne National Lab.(ANL), Argonne, IL, 2022.
[12] Chaugule, Pawan, et al. "Investigating Various Failure Models on Commercial Silicon Carbide." *SolarPACES Conference Proceedings*. Vol. 1. 2022.
[13] M.C. Messner, and B. Barua. "A fast tool for receiver life estimation and design." *AIP Conference Proceedings*. Vol. 2445. No. 1. AIP Publishing, 2022.
[14] M.C. Messner, et al., “*srlife: A Fast Tool for High Temperature Receiver Design and Analysis,”* (No. ANL-22/29). Argonne National Lab.(ANL), Argonne, IL, 2022. (https://doi.org/10.2172/1871331)
[15] Barua, Bipul, and Mark C. Messner. "Fast heuristics for receiver life estimation and design." *AIP Conference Proceedings*. Vol. 2815. No. 1. AIP Publishing, 2023.